

# Sub-seasonal teleconnections between convection over the Indian Ocean, the East African long rains and tropical Pacific surface temperatures

N. Vigaud,\* B. Lyon and A. Giannini

*International Research Institute for Climate and Society, Earth Institute at Columbia University, New York, USA*

**ABSTRACT:** Since 1999, the increased frequency of dry conditions over East Africa, particularly during the March–May (MAM) season, has heightened concerns in a region already highly insecure about food. The underlying mechanisms, however, are still not yet fully understood. This article analyses a proxy for daily convection variations over a large region encompassing East Africa and the whole Indian Ocean basin by applying a cluster analysis to more than 30 years of daily outgoing longwave radiation (OLR). Focusing on the MAM season to investigate relationships with East African long rains, four recurrent convection regimes associated with wet/dry conditions in East Africa are identified. Interestingly, all four regimes are related to western/central Pacific sea surface temperatures (SSTs) and rainfall. Wet regimes are associated with cool and dry/warm and wet conditions over the Maritime Continent (MC)/tropical Pacific east of the date line. Dry regimes exhibit opposite SST/rainfall dipole patterns in the Pacific compared to wet regimes, with the Indian Ocean found to modulate impacts on East African rainfall. Significant relationships between off-equatorial warming in the west Pacific and a more frequent dry regime in May since 1998–1999 suggest an earlier onset of the monsoon and Somali jet, consistent with the recent abrupt shift observed in East African long rains and their modulation at multi-decadal time scales of the Pacific.

**KEY WORDS** East African long rains; ENSO; sub-seasonal climate variability

*Received 24 November 2015; Revised 8 March 2016; Accepted 31 March 2016*

## 1. Introduction

Due to large topographical variations over the region, the East African climate exhibits great spatial heterogeneity (Hession and Moore, 2011; Liebmann *et al.*, 2012; Lyon, 2014). The annual rainfall cycle is generally bimodal across much of the region, where local climate is tightly associated with the latitudinal migration of the Intertropical Convergence Zone (ITCZ). The ITCZ particularly modulates the north-/south-east trades during the southern/northern summer, respectively, resulting in two rainy seasons phased with the transitions between the winter and summer monsoons: the ‘short’ and ‘long’ rains, with maximum rainfall from October to December (OND) and from March to May (MAM), respectively. Most of the agriculture is rainfed; thus, local populations are vulnerable to climatic variations, making East Africa a highly food-insecure region (Shukla *et al.*, 2014). Indeed, the recent failure of both the long and short rains in 2010–2011 (Lyon and DeWitt, 2012) resulted in severe drought, contributing to a humanitarian crisis impacting millions of people. To date, several investigations have documented a recent decline in long rains since 1998–1999 (Lyon and DeWitt, 2012; Omondi *et al.*, 2013;

Pricope *et al.*, 2013; Funk *et al.*, 2014a) and even earlier in some areas relying heavily on the MAM rainy season (Verdin *et al.*, 2005; Viste *et al.*, 2011; Williams and Funk, 2011; Omondi *et al.*, 2013; Afifi *et al.*, 2014; Liebmann *et al.*, 2014; Nicholson, 2014). Additional studies provide evidence that East African long rains shifted abruptly through tropical Pacific SST forcing (Lyon and DeWitt, 2012; Lyon, 2014; Yang *et al.*, 2014), while a recent warming trend in the Pacific warm pool has also been associated with a stronger Walker circulation, driven primarily by the tropical Pacific SST gradient (Funk *et al.*, 2014a; Hoell and Funk, 2014). Less is known, however, at sub-seasonal time scales despite the need to better understand rainfall processes and their variability (Camberlin and Philippon, 2002; Camberlin and Okoola, 2003), especially in light of the recent drying observed. Berhane and Zaitchik (2014), for instance, have identified sub-seasonal associations between the Madden-Julian oscillation (MJO) and East African long rains variability that could operate through diverse mechanisms, including modulations of the Somali low-level jet and, at different lead times, illustrations of the potential for regional climate predictability within the season.

Seasonal variations in East African rainfall have been examined in several earlier studies, with associations identified with southwest Indian Ocean (IO) SSTs (Walker, 1990; Mason, 1995; Behera *et al.*, 2005) and El Niño Southern Oscillation (ENSO) (Beltrando, 1990; Beltrando

\* Correspondence to: N. Vigaud, International Research Institute for Climate and Society, Earth Institute at Columbia University, Hogan Hall, 2910 Broadway, NY 10025, USA. E-mail: nicolas.vigaud@gmail.com

and Camberlin, 1993; Goddard and Graham, 1999; Indeje *et al.*, 2000; Nicholson, 2015). The influence of ENSO on East African short rains (in October–December or OND) appears to be modulated by its control on IO SSTs. Goddard and Graham (1999) report that when low-level wind anomalies during El Niño/La Niña events result in a warmer/cooler western IO, and thus an anomalous zonal SST gradient across the IO basin, rainfall is reduced/enhanced in the east and conversely increased/decreased over the adjacent East African region in the west. By contrast, less is known regarding ENSO teleconnections during the long rains season (MAM) (Ogalo, 1988; Ogalo *et al.*, 1988; Hastenrath *et al.*, 1993; Philipps and McIntyre, 2000). Recently, however, Liebmann *et al.* (2014) found substantial relationships in SST-forced ECHAM5 simulations between the recent March–May drying in East Africa and an increased SST zonal gradient between the west and central Pacific. This study reports that this has strengthened the convection over the Maritime Continent (MC) and generated anomalous westerlies over the equatorial IO, with associated subsidence over the western equatorial IO.

At sub-seasonal time scales, there is limited evidence of teleconnections between East African long rains and ENSO (Mutai and Ward, 2000; Moron *et al.*, 2013). Mutai and Ward (2000) found some influence in May but not in the prior March and April months, while Moron *et al.* (2013) suggested a greater spatial coherence for March than for April and May. In addition, Pohl and Camberlin (2006a, 2006b) and, more recently, Berhane and Zaitchik (2014) reported significant influences of the MJO on both long and short rains, but with contrasted impacts between highlands and coastal regions.

Despite recent advances regarding East African long rains variability, the atmospheric mechanisms responsible for the sub-seasonal development of rain-producing convective systems over the region, as well as their variability in both time and space, are not yet fully understood. Regional convection is known to organize within the Walker circulation, characterized by ascending/subsiding branches over the MC/East Africa, respectively. In this sense, convection variability over East Africa at sub-seasonal time scales can be seen as part of a larger, basin-wide pattern that we consider here by applying a clustering of daily outgoing longwave radiation (OLR) for a domain encompassing central, eastern and southern Africa and the Indo-Pacific. Therefore, the main objective of this study is to characterize recurrent daily OLR patterns over the larger East Africa–IO region in order to examine the related atmospheric anomalies conducive to such preferential regimes in relation to East African rainfall in MAM. A second objective is to investigate how sub-seasonal variability in convection is related to inter-annual time scales and large-scale teleconnections to further explain the recent long rains decline.

The paper outline is as follows. The method and data are presented in Section 2. Results from the cluster analysis are discussed in Section 3, with their relationships to rainfall and associated atmospheric circulation anomalies

presented in Section 4. Large-scale teleconnections are examined in Section 5 alongside the recent abrupt shift towards drier conditions in East Africa since 1999. Discussions and conclusions are summarized in Section 6.

## 2. Data and methods

### 2.1. Observations and atmospheric data

Tropical convection is examined using daily OLR (Liebmann and Smith, 1996) produced by the National Oceanic and Atmospheric Administration (NOAA) and available on a regular  $2.5^\circ \times 2.5^\circ$  grid from 1979 to present.

Gridded daily rainfall estimates from the Climate Hazards group InfraRed Precipitation, with a Station dataset (CHIRPS) developed at the University of California at Santa Barbara (UCSB) Climate Hazards Group (CHG) in collaboration with the U.S. Geological Survey (USGS) Earth Resources Observation and Science (EROS) centre, (Funk *et al.*, 2014b, 2015b) are utilized for examining weather regime relationships to rainfall by compositing. These land-only data are at a  $0.05^\circ$  spatial resolution and provide daily rainfall information for the 1981–2012 period. Despite including satellite information, CHIRPS is one of the few available datasets covering the whole sub-continent at daily time scales that has data back from the 1980s. A box extending over  $10^\circ\text{S}–12^\circ\text{N}$ ;  $30^\circ–52^\circ\text{E}$ , including land areas, is exclusively used to define an index of East African rainfall for the MAM season (Figure 1). This index is significantly correlated with grid point rainfall locally (according to Monte-Carlo simulations), thus justifying its use to characterize rainfall variability for the whole region (Figure 1). To place the recent evolution of East African long rains in the context of the long-term decline discussed in several studies (Funk *et al.*, 2008, 2014a; Williams and Funk, 2011; Lyon and DeWitt, 2012; Hoell and Funk, 2014; Lyon, 2014), precipitation estimates from the Global Precipitation Climatology Center (GPCC) version 6 at a half degree spatial resolution are also averaged over the same East African box from 1901 to 2010. To this end, the later dataset is complemented with the recently released Centennial Trends precipitation estimates developed by scientists at UCSB and Florida State University (FSU) and offers seasonal rainfall products over a  $0.1^\circ$  grid covering  $15^\circ\text{S}–18^\circ\text{N}$ ;  $28^\circ–54^\circ\text{E}$  from 1900 to 2014 (Funk *et al.*, 2015a). In addition, the Global Precipitation Climatology Project (GPCP) version 2.2 (Adler *et al.*, 2003) dataset, offering monthly rainfall estimates at  $2.5^\circ \times 2.5^\circ$  spatial resolution from 1979 to present, is used to build global composites for MAM seasons marked by maximum/minimum number of occurrences of each convection regime.

Daily atmospheric fields from the NCEP-DOE II re-analyses (NCEP2 in the following), produced jointly by the National Centers for Environmental Prediction (NCEP) and the U.S. Department Of Energy (DOE), at a  $2.5^\circ \times 2.5^\circ$  horizontal resolution (Kanamitsu *et al.*, 2002), are used to examine relevant atmospheric circulation features over the 1979–2013 period. Moisture fluxes from

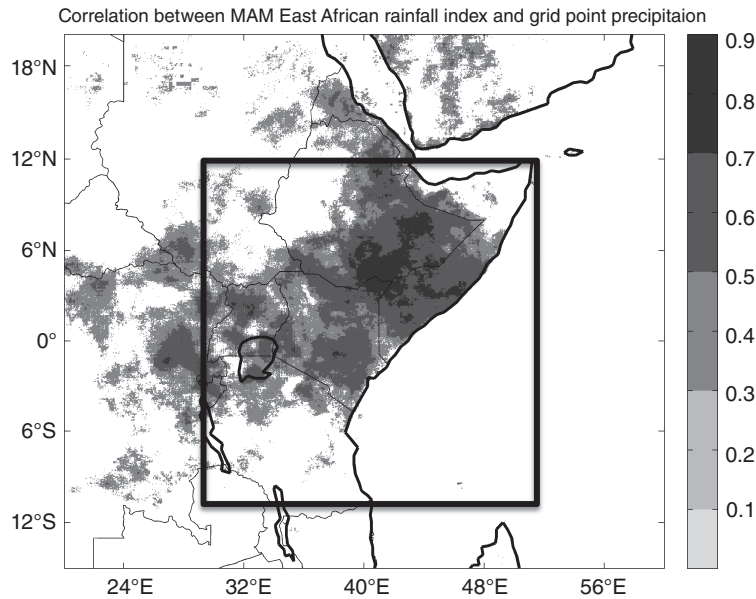


Figure 1. Correlation between MAM East Africa rainfall index averaged over  $10^{\circ}\text{S}–12^{\circ}\text{N}$ ;  $30^{\circ}–52^{\circ}\text{E}$ ] (black box) and grid-point precipitation from CHIRPS dataset for the 1981–2012 period. The scores presented are significant at the 95% confidence level using Monte-Carlo simulations.

the re-analyses were computed following earlier studies (Vigaud *et al.*, 2007, 2009). At a given level, the horizontal moisture flux can be defined as

$$\vec{Q}_{lvl} = q_{lvl} \cdot \vec{v}_{lvl} \quad (1)$$

where  $q_{lvl}$ ,  $\vec{v}_{lvl}$  are the specific humidity and horizontal velocities at a given tropospheric level, respectively. Consequently, moisture flux convergence is calculated from the zonal and meridional moisture flux components. At monthly or seasonal time scales, temporal variations of precipitable water in a given volume can be considered small, leading to the following approximation (Peixoto and Oort, 1992)

$$-\text{div}\vec{Q} = P - E \quad (2)$$

When integrated over the whole air column, water vapour convergence is associated with an excess in precipitation ( $P$ ) over evaporation ( $E$ ), while the reverse is associated with divergence.

The relationships between each identified convection regime and sea surface temperatures (SSTs) in the different oceanic basins are assessed using the NOAA Optimum Interpolation SST version 2 (OISST) dataset consisting of daily values at a quarter of a degree spatial resolution, which were aggregated to the MAM season from 1982 to 2009 (Reynolds *et al.*, 2007).

## 2.2. Dynamical clustering approach

In this paper, convective activity is examined by identifying recurrent spatial patterns using a methodology that has been previously applied successfully to the southern African region (Fauchereau *et al.*, 2009; Vigaud *et al.*, 2012). Daily OLR anomalies (obtained by subtracting the mean annual cycle) are input into an objective classification scheme that makes use of  $k$ -means clustering

(Michelangeli *et al.*, 1995; Cheng and Wallace, 2003) over the domain  $40^{\circ}\text{S}–30^{\circ}\text{N}$ ;  $0^{\circ}–120^{\circ}\text{E}$ , encompassing central, eastern and southern Africa as well as the Indo-Pacific. Using such a design, to which the sensitivity of the results have been tested, the approach presented here aims to identify convection regimes prevailing broadly over the IO and neighbouring regions such as East Africa, where their impact on local rainfall will ultimately be examined. An EOF analysis is first performed on the data correlation matrix, and the first 11 PCs, explaining 27.6% of the variance, are retained. Although the results are not dependent on the percentage of variance retained (Fauchereau *et al.*, 2009), a third of the total variance is a significant amount when compared to the large size of the study domain stretching across the entire IO and ensures that this decomposition succeeded in separating the signal in large-scale patterns from the background noise. The Euclidean distance is then used to measure similarities between daily OLR patterns and a given regime. The robustness of regime partitions is tested following previous studies (Michelangeli *et al.*, 1995; Moron and Plaut, 2003; Fauchereau *et al.*, 2009; Vigaud *et al.*, 2012); 100 different partitions of daily OLR anomaly patterns are performed, each time with a different randomly drawn initialization. A measure of the dependence between the final partition on the initial random draw consists of comparing several final partitions for a given number of regimes  $k$ . The average similarity within the 100 sets of regimes is then measured by a classifiability index (Cheng and Wallace, 2003), which evaluates the similarity within the 100 sets of regimes (i.e. its value would be exactly 1 if all the partitions were identical), and is compared to confidence limits from a red-noise test (applied to Markov-generated red-noise data) based on 100 samples of the same length, providing 100 values of the classifiability index. The operation is repeated for  $k$ , varying from 2 to 10.

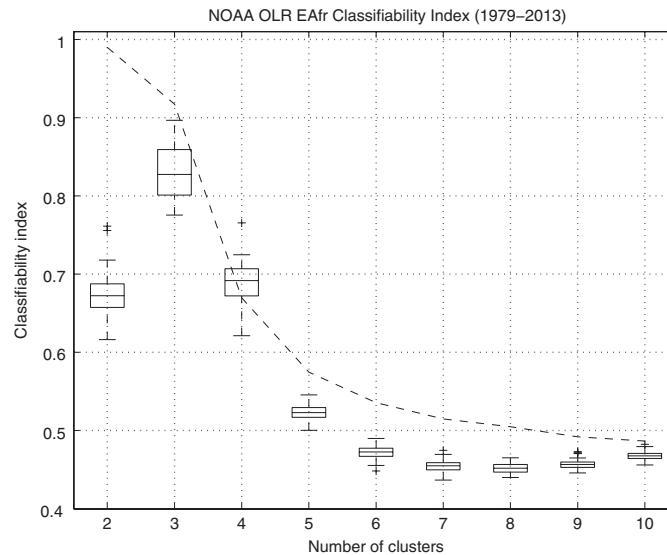


Figure 2. Classifiability index as a function of the number of regimes  $k$  (boxes). The 95% level of significance (dashed line) is computed according to a first-order Markov process.

Results from composites related to each daily OLR regime are tested at the 95% confidence level using a Student's  $t$ -test.

### 3. Daily OLR regimes over East Africa and the Indian Ocean

To identify daily convection regimes during the long rains over the 1980–2013 period,  $k$ -means clustering is applied to MAM NOAA daily OLR anomalies following the methodology described in Section 2.2. The corresponding  $k$ -means classifiability index (Figure 2) exhibits a significant peak for  $k = 4$ , while larger numbers of regimes are not statistically significant. Therefore, the partition of the four regimes is chosen as the one giving the most compact summary.

MAM daily OLR anomaly patterns associated with the four regimes identified are presented in Figure 3. The first four classes are characterized by different patterns of maximum OLR anomalies. During regime 1, convection is increased over East Africa and along a band stretching southeastward towards Australia. Convection is reduced over the MC. Regime 2 is also characterized by an overall increase of convection over East Africa and much of the continental interior. Decreased convection is seen over the eastern IO. During regime 3, convection is somewhat reduced over East Africa, with significant OLR anomalies but weak in magnitude, and are enhanced over the eastern IO, showing stronger anomalies of the opposite sign. Finally, regime 4 displays a more pronounced reduction of convection over East Africa, while it is enhanced over the west Pacific. Overall, regime 1 (4) represents the most (least) convective conditions over East Africa.

The number of transitions between the four OLR regimes over the full analysis period is provided in Table 1. The highest values are found along the diagonal, suggesting

the persistence of each regime at daily time scale. Consistently, no significant relationship is found between the different regimes, supporting the idea that these classes are independent and have no preferential sequence. As indicated by the low variations of percentages along the diagonal, there is not a large difference in the mean persistence of each regime, that is, about 3, 4, 4.5 and 3.75 days for regimes 1, 2, 3 and 4 respectively. However, there is a substantial spread in the duration of their respective episodes, an aspect which is discussed later in Section 5.1 at inter-annual time scales (see Figure 9).

The number of occurrences of each regime is broken down by month in Table 2. Overall, regime 1 tends to occur throughout the entire season but shows maximum occurrences in April. Regime 2 occurs preferably during the first half of the season, with the highest number of occurrences in March. Regimes 3 and 4 are both characterized by a maximum number of occurrences in May and outnumber regimes 1 and 2 every month. The MAM period thus appears to be dominated by OLR regimes that are not favourable to convection processes over East Africa, a result consistent with the climatologically divergent flow over the region (Yang *et al.*, 2014). By contrast, regime 2, and to a lesser extent regime 1, corresponds to conditions favourable to the development of rainfall-producing systems during the long rains.

### 4. Relationships to East African long rains and associated dynamics

The relationships between daily OLR regimes and East African rainfall are examined through composites of rainfall anomalies from CHIRPS, as presented in Figure 4. The rainfall anomaly patterns for regimes 1, 2 and 4 are statistically significant and spatially coherent, much less so for regime 3. NOAA OLR comes from polar-orbiting satellites, while CHIRPS rainfall estimates contain remote

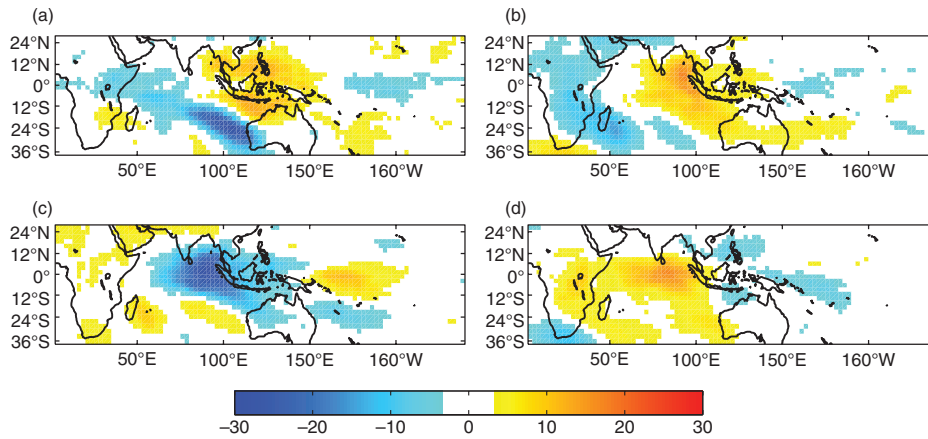


Figure 3. Mean MAM NOAA daily OLR (in  $\text{W m}^{-2}$ ) for the four OLR regimes identified. (a) Class 1, (b) Class 2, (c) Class 3 and (d) Class 4. Only the grid points for which anomalies are significant at the 95% confidence level of a Student's  $t$ -test are displayed.

Table 1. Contingency tables between the four daily OLR classes from NOAA. The scores (in %) indicated with a star are significant at the 99.9% level of  $\chi^2$  test.

OLR classes	Class 1	Class 2	Class 3	Class 4
Class 1	68.05*	05.52	08.56	05.84
Class 2	11.91	74.48*	07.19	09.84
Class 3	09.83	05.64	76.37*	12.24
Class 4	10.21	14.36	07.88	72.08*

Table 2. Numbers of monthly occurrences of the four NOAA daily OLR classes.

	Class 1	Class 2	Class 3	Class 4
March	173	301	308	272
April	194	276	258	292
May	167	250	319	318
Total	534	827	885	882

sensing information from geostationary satellites. Even if no in-situ data is used in this analysis, OLR and rainfall estimates may be consequently considered independent. In this sense, the above patterns suggest that the OLR clustering successfully isolated regimes associated with significant day-to-day rainfall variability during the East African long rains. In order to further document these relationships, the associated atmospheric circulation anomalies are investigated through composites of NCEP2 850 hPa moisture fluxes/convergence. As will be shown, each daily OLR regime is related to distinct large-scale circulation anomalies, further illustrating a successful partitioning of daily OLR into recurrent atmospheric conditions prevailing over the region.

Regimes 1 and 2 are associated with wet conditions over East Africa and tend to recur more frequently in April and March, respectively. Given the strong seasonality of the regional atmospheric circulation from March to May, Figures 5 a, c and e display moisture fluxes and convergence anomalies associated with regime 1 for each month separately, along with the seasonal mean that will

be emphasized. For the MAM season (Figure 5(g)), an enhanced moisture flux from the northern IO into East Africa is identified in the equatorial zone. Consistent with the dipole-like rainfall anomaly pattern associated with this regime (Figure 4(a)), moisture flux divergence is generally seen over the MC and western Pacific region. Regime 2 is characterized by broad easterly moisture flux anomalies across the IO at equatorial latitudes into East Africa (Figure 5(h)) with enhanced moisture convergence anomalies over the region. Similar to regime 1, moisture flux divergence is again seen over the MC but with a pattern extending westward over the eastern IO. These results corroborate earlier studies that described anomalous inflow from the Arabian Sea in wet Aprils (Beltrando, 1990).

Similar to Figure 5, Figure 6 presents monthly moisture/fluxes and convergence anomalies but for regimes 3 and 4, the dry regimes in East Africa. Because regime 3 is noticeably the regime associated with the least coherent rainfall anomalies in East Africa (Figure 4(c)), consistent with weaker OLR anomalies over the region (Figure 3(c)), it will be the least discussed in the following. However, a systematic feature persisting from March to May consists of westerly moisture flux anomalies across the whole IO at equatorial latitudes, sustaining local moisture divergence over coastal regions from southern Tanzania to the Greater Horn (Figure 6(b), (d) and (f)). Worth noting, the peak of long rains (in April) is when regime 3 is the most active (Table 2), a period dominated by internal chaotic atmospheric variations (Ogallo, 1988; Camberlin and Philippon, 2002), which could explain the poor significance of related rainfall anomalies. Regime 4 features an enhanced moisture flux divergence over East Africa associated with an anomalous moisture flux somewhat opposite to regime 2 over the IO (Figure 6(h)). These anomalies, however, are clearly pronounced only during May (Figure 6(f)), when regime 4 preferentially develops (Table 2). These findings are consistent with earlier studies reporting stronger easterlies over equatorial Africa up to mid-tropospheric levels during dry years and dry spells within the long rains (Okoola, 1999; Camberlin and Philippon, 2002). Such timings further suggest that the southerly/westerly

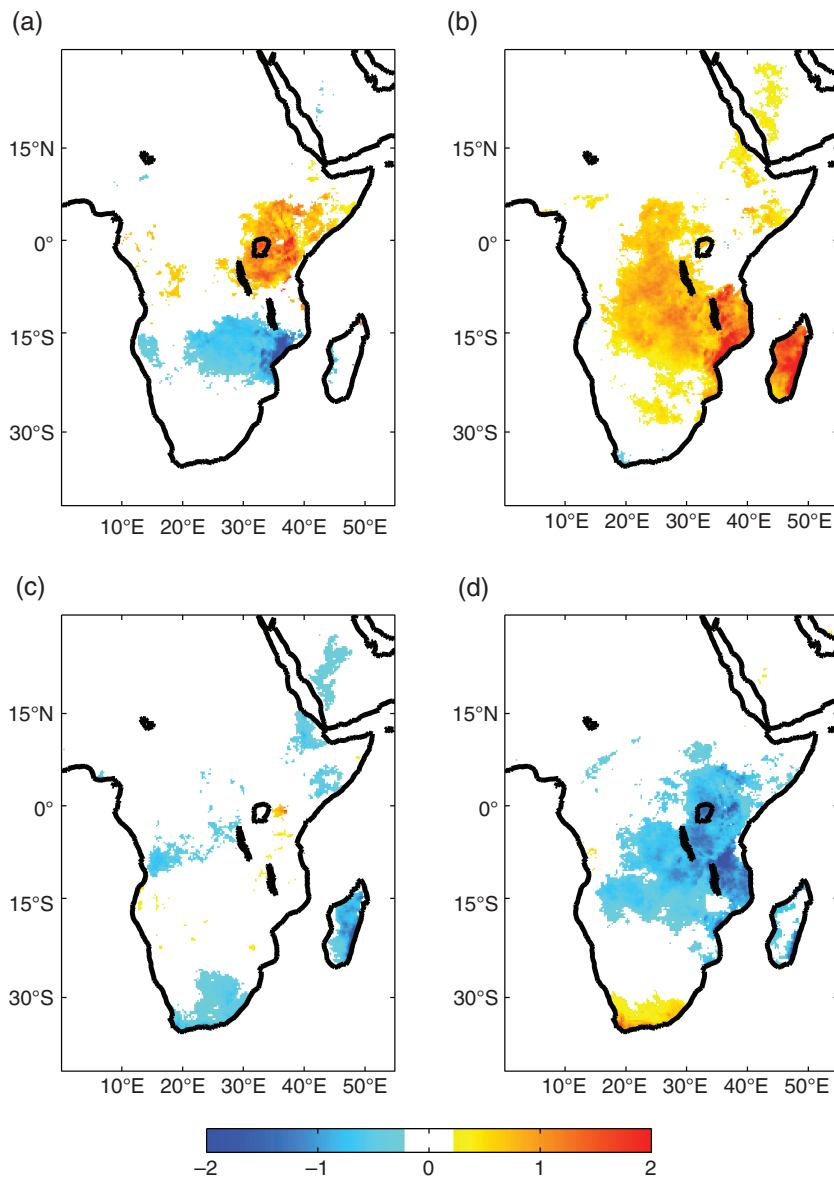


Figure 4. Mean CHIRPS daily rainfall anomalies for the four daily OLR classes occurrences. (a) Class 1, (b) Class 2, (c) Class 3 and (d) Class 4. Only the grid points for which anomalies are significant at the 95% confidence level of Student's *t*-test are displayed (in  $\text{mm day}^{-1}$ ).

anomalies prevailing along the East African coast/off the Greater Horn to the northeast over the IO, and sustaining moisture divergence over East Africa north of the Equator (Figure 6(h)), can be related to the establishment of the Somali *jet* along the East African coast. The end of East African long rains is thus concomitant with the start of the Indian monsoon, as described by Vizzy and Cook (2003), Riddle and Cook (2008) and others.

## 5. Inter-annual variability and the recent decline of the East African long rains

### 5.1. Year-to-year variability in daily OLR regimes frequency

As in earlier studies (Lyon and DeWitt, 2012; Lyon, 2014), we computed MAM East African rainfall indices for land areas over  $10^{\circ}\text{S}–12^{\circ}\text{N}$ ;  $30^{\circ}–52^{\circ}\text{E}$  from daily

CHIRPS estimates and monthly GPCC data along with corresponding anomalies (1980–2009 base period). These are shown in Figure 7. Rainfall anomalies for individual months within MAM (Figure 7(a)) display out-of-phase variability between March, April and May, suggesting different mechanisms between the beginning and the end of the season. Figure 7(b) presents a longer time-series for GPCC and Centennial Trends estimates, placing the recent East African long rains decline in a historical context. As discussed in previous studies (Funk *et al.*, 2008, 2014a; Williams and Funk, 2011; Lyon and DeWitt, 2012; Hoell and Funk, 2014; Lyon, 2014; Yang *et al.*, 2014), East Africa has experienced a substantial precipitation reduction, particularly during the post-1998 period when the west Pacific has been anomalously warm, and central regions of the basin are cool (Lyon and DeWitt, 2012; Funk *et al.*, 2014a; Lyon, 2014). Figure 7(b) illustrates the intensification of this decline after 1998 likely due to both

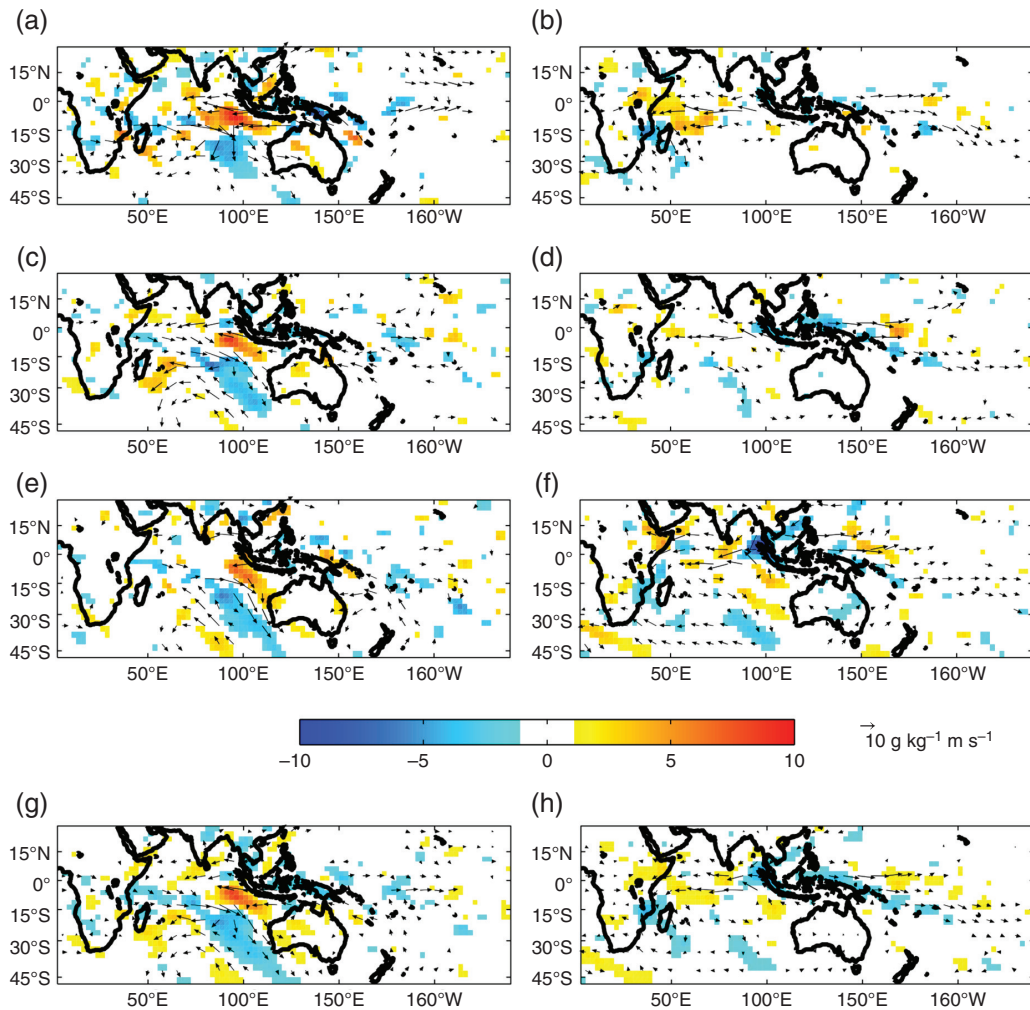


Figure 5. Monthly (a–f) and seasonal (g, h) mean NCEP2 daily 850 hPa moisture fluxes (vectors in  $\text{g kg}^{-1} \text{m s}^{-1}$ ) and convergence (red/blue shadings indicating anomalous convergence/divergence in  $\text{g kg}^{-1} \text{s}^{-1}$ ) anomalies for the wet OLR regimes (1 and 2). Only the grid points for which anomalies are significant at the 95% confidence level of a Student's  $t$ -test are displayed.

the west-central Pacific gradient and PDO-like variability as recently demonstrated (Liebmann *et al.*, 2014; Lyon, 2014; Lyon *et al.*, 2014).

Figure 8 displays the differences between the number of occurrences of each regime (for the MAM season exclusively) and associated mean values computed for the 30-year climatology. During MAM, mean occurrences of regimes 1, 2, 3 and 4 are, respectively, about 14, 23, 27 and 28 days, consistent with results from Table 1. The number of days during which the different regimes occur varies substantially from one year to another. To examine how variations in regime occurrence are related to seasonal rainfall, the five driest/wettest MAM seasons (1984, 1992, 2000, 2008 and 2009 versus 1981, 1985, 1987, 1989 and 1990, respectively) from Figure 7(a) are also indicated in Figure 8. All of the wettest years are found before 1999, along with two of the five driest years in general agreement with earlier studies reporting the recent decrease in East African long rains since then (Lyon and DeWitt, 2012; Lyon, 2014).

Three wet years out of five (1981, 1987 and 1989) are characterized by an increased number of regime 1

occurrences (Figure 8(a)), while three other years out of the same set (1981, 1985 and 1989) are associated with more frequent occurrences of regime 2 (Figure 8(b)). Moreover, wet years 1981, 1987 and 2000 coincide with a reduction of dry regimes 3 and 4 occurrences (Figure 8(c) and (d)). Four of the five driest years (1984, 2000, 2008 and 2009) are related to a decrease in the number of occurrences of wet regime 1. The dry years of 1984, 1992, 2000 and 2008 (as well as 2011) also show a decrease in the frequency of occurrences of wet regime 2. Four of the driest years (1984, 1992, 2000 and 2008) correspond to increased occurrences of dry regime 3, the 30-year sample chosen for rainfall compositing, being heavily weighted by year 2000, associated with strong La Niña conditions. Increased occurrences of regime 3 in 1999, 2000, 2008 all coincide with La Niña episodes. Finally, it is found that the driest years (except 2000), as well as the recent MAM 2011 severe drought, are all related to an almost systematic increase in dry regime 4 occurrences (Figure 8(d)).

The main durations of episodes associated with the four regimes are shown in Figure 9 for each year of the 1979–2013 period. Overall, regimes 1, 2 and 4 do

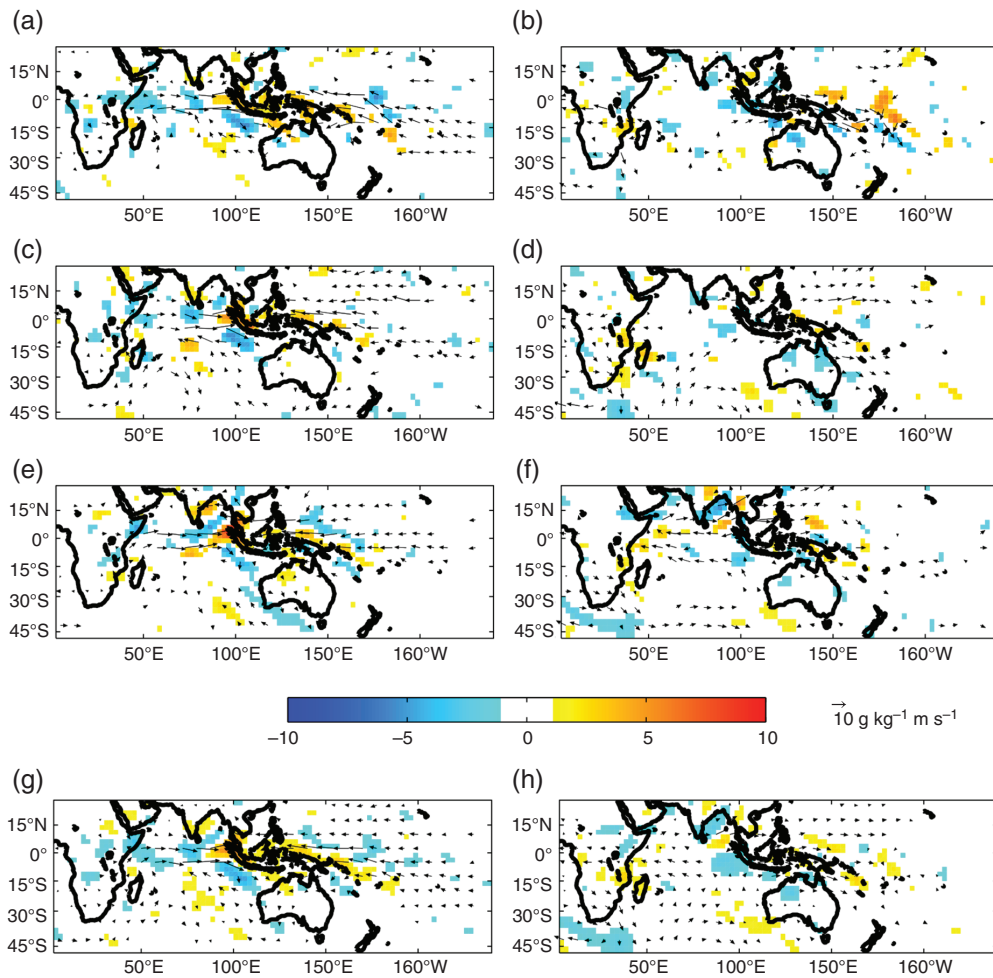


Figure 6. Monthly (a–f) and seasonal (g, h) mean NCEP2 daily 850 hPa moisture fluxes (vectors in  $\text{g kg}^{-1} \text{m s}^{-1}$ ) and convergence (red/blue shadings indicating anomalous convergence/divergence in  $\text{g kg}^{-1} \text{s}^{-1}$ ) for the dry OLR regimes (3 and 4). Only the grid points for which anomalies are significant at the 95% confidence level of a Student's *t*-test are displayed.

not show variations as large as regime 3. The latter is marked by maximum durations in 1988, 1999, 2000 and 2008, all corresponding to cold phases of ENSO. Interestingly, an increase in regime 3 persistence is noticeable after 1998–1999, contrasting with a decrease for wet regime 1.

As expected, the recent decline in East African rainfall was accompanied by more/less frequent dry/wet regimes since 1999. Because such regime partitioning is also valid for the recent 2011 drought, the different regime relationships to large-scale SSTs will be examined in the following section, together with their modulations since 1999.

## 5.2. Relationships to large-scale SSTs

Enhanced occurrences of regime 1 are significantly related to an SST pattern having a typical El Niño signature in the Pacific (Figure 10(a)). It is accompanied by a V-like cooling pattern in the western extratropics of the basin, similar to the West Pacific Warming Mode (WPWM) reported by Funk and Hoell (2015), the overall structure of the anomalies being also consistent with that of the recent SST changes identified by Lyon and DeWitt

(2012). Such a combination of multi-annual ENSO and trend component in the west Pacific could thus explain the strong non-stationarity shown in Figure 8(a) for this regime. GPCP precipitation composites for regime 1 (Figure 10(b)) display a strong precipitation dipole with enhanced/reduced rainfall over the central/west Pacific, while rainfall is also enhanced over the central IO. This further suggests an increase in the number of occurrences of regime 1 during El Niño years. The circulation anomalies from Figure 5(g) also bear similarities to the northeast-ward shift of the tropical–temperate trough over southern Africa/southwest IO, again typical of ENSO modulations (Vigaud *et al.*, 2007, 2012).

Regime 3 composites (Figure 10(e) and (f)) display almost opposite anomalous SST and rainfall patterns to those from regime 1. SST anomalies are less pronounced for regime 3; nevertheless, changes in the west-central SST gradient are marked by the strongest and most significant loadings across the tropical Pacific, where rainfall anomalies are also the greatest. The latter consists of enhanced/reduced precipitation from India to the MC/over the central Pacific and IO, a pattern similar to La Niña impacts.

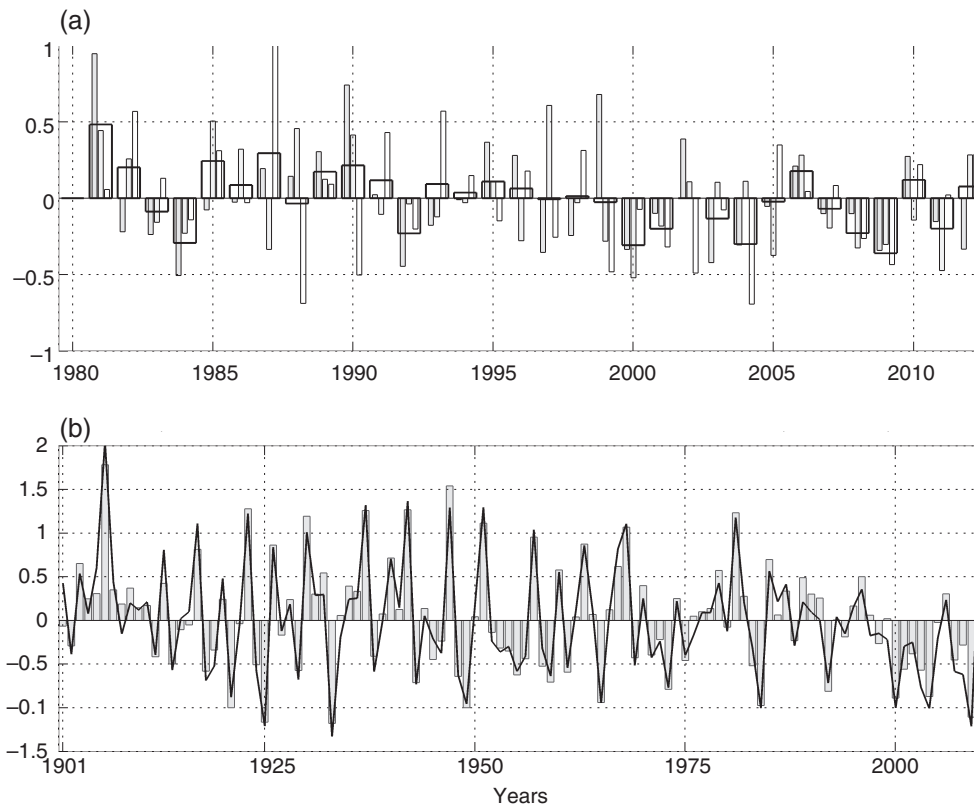


Figure 7. (a) Mean MAM CHIRPS rainfall standardized anomalies (thick black) averaged over an East African box ( $[10^{\circ}\text{S}–12^{\circ}\text{N}; 30^{\circ}–52^{\circ}\text{E}]$ ) together with these for March, April and May (grey bars) over the 1980–2012 period (in  $\text{mm day}^{-1}$ ); (b) similar plot but for GPCC (grey bars) and Centennial Trends (black line) rainfall standardized anomalies over the 1901–2010 period (in  $\text{mm day}^{-1}$ ).

Over the Pacific Ocean, regime 2 is associated with an SST anomaly pattern generally featuring an off-equatorial signature in the Pacific (Figure 10(c)). Precipitation anomalies for regime 2 differ from regime 1, showing enhanced rainfall in the central equatorial Pacific and reduced drying over the MC. Over the IO, there is more of an east–west dipole structure (Figure 10(d)).

Finally, Figure 10(g) displays regime 4 patterns of SST anomalies generally opposite to regime 2, with significant negative SST anomalies in the North Pacific, positive anomalies arching from the MC into the extratropics in both the Northern and Southern Hemispheres. The related rainfall anomalies (Figure 10(h)), similar to regime 3, exhibit enhanced rainfall over the MC and northeast-wards/southeast-wards in the subtropics of both hemispheres, with a significant reduction in precipitation over the central Pacific. SST and rainfall anomalies in the IO for this regime tend to show enhanced anomalies compared to those found for regime 3. Interestingly, a similar MC-central Pacific SST gradient to that seen in Figure 10(e) for regime 3, does not seem to translate into substantial rainfall anomalies in East Africa (Figure 4(c)). This suggests that East African rainfall variations in MAM are sensitive to the specific configuration of SST anomalies in a nonlinear way. Conversely, different SST forcing patterns seem to be associated with similar large-scale rainfall anomalies that consistently and significantly associate wet/dry conditions in East Africa with

reduced/enhanced rainfall in the eastern equatorial IO near the MC. Regime 2 further emphasizes the importance of this east IO rainfall linkage, suppressed east IO rainfall being concomitant with enhanced precipitation over East Africa (Figure 10(d)). Such relationships are in agreement with earlier studies from Funk *et al.* (2008), who noted that enhanced convection over the MC is generally associated with enhanced subsidence over East Africa primarily driven by west-central Pacific gradients (Williams and Funk, 2011; Lyon and DeWitt, 2012), results that have been confirmed by Liebmann *et al.* (2014) using GCM experiments.

Except regime 3, all regimes are characterized by significant relationships to west-central Pacific SST gradients in the tropics, while dry regime 4 is also associated with off-equatorial Pacific SSTs near Hawaii, which are part of the WPWM (Funk and Hoell, 2015). Finally, Figures 8 and 10 illustrate the fact that the Indo-Pacific convective structure integrates complex SST signals to ultimately produce a consistent and persistent drying tendency over East Africa, as shown in Figure 7.

### 5.3. The recent shift in East African long rains

To document the recent abrupt shift in East African long rains since 1999, the number of occurrences of each regime is shown in Table 3 for the 1988–1998 and 1999–2009 periods together with their differences for individual months. Table 3 emphasizes substantial changes

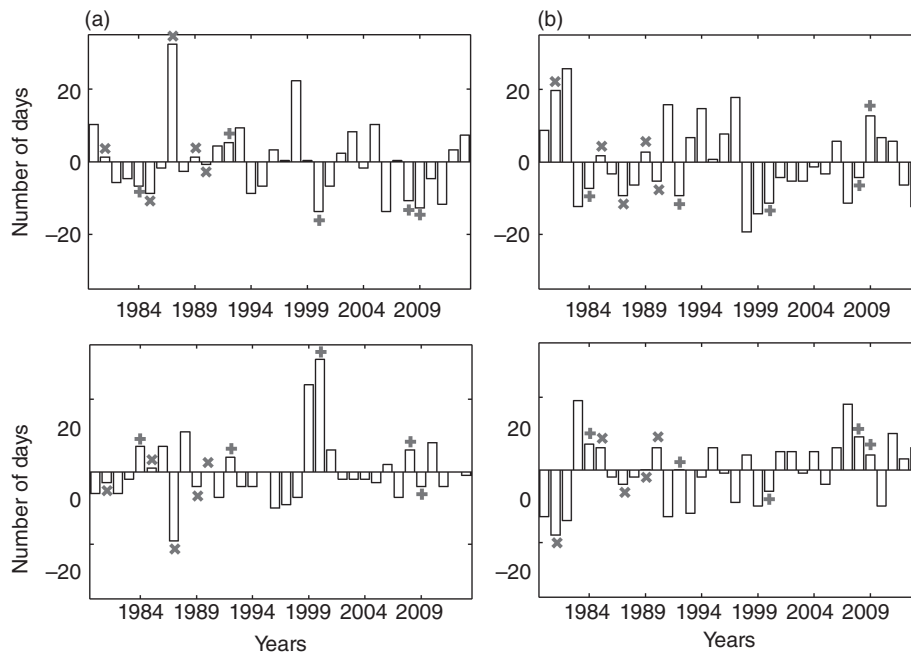


Figure 8. Time series of the differences in number of days spent in each regime during each MAM season compared to the long-term mean. (a) Class 1, (b) Class 2, (c) Class 3, and (d) Class 4. The +/× symbols indicate the five driest/wettest years, respectively, according to the East African index from figure 7.

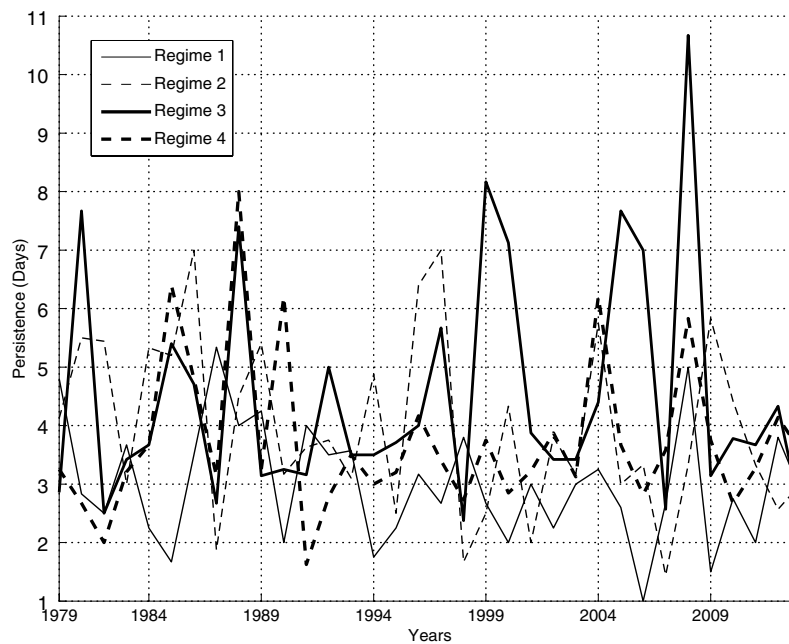


Figure 9. Mean persistence (in days) of each daily OLR regime by year over the 1979–2013 period.

in the monthly occurrences of each convection regime for the post-1999 period; the maximum occurrences of regimes 2 and 4 particularly seem to have shifted from March to May, while regime 3 became more frequent in March instead of May before 1999. After 1999, dry regimes prevail even more significantly at the beginning and end of the season, which is not the case earlier on, especially in March. Maximum increases in March and May could further indicate a shrinking of the seasonal cycle. Seasonal differences for each regime between the

pre- and post-1999 periods exhibit a reduction in the occurrence of wet regimes (1 and 2), with more events related to dry regimes (3 and 4). The time-series presented in Figure 8(b) and (d) clearly show a shift in 1998–1999 associated with regimes 2 and 4, marked by almost exclusively enhanced/reduced number of occurrences, which is consistent with an enhancement of the MC-central Pacific SST gradient (cold–warm/warm–cold) described earlier. In the case of regime 4, the significant linkage with enhanced rainfall over the MC further supports its

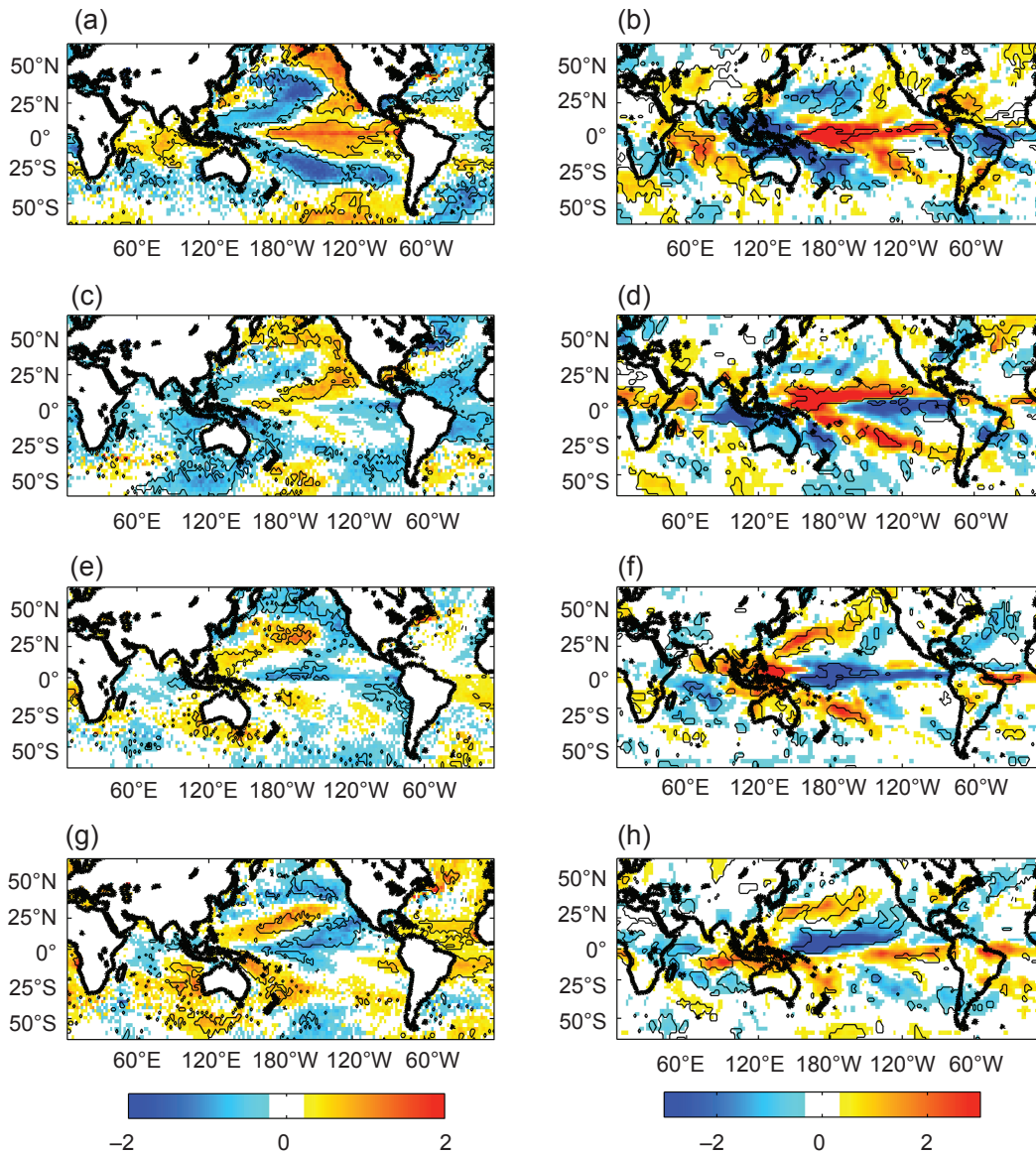


Figure 10. Composites of OISST (in  $^{\circ}\text{C}$ ) and GPCP rainfall (in  $\text{mm day}^{-1}$ ) differences for the five largest/smallest number of occurrences of each daily OLR regime from Figure 8. (a) Class 1 OISST, (b) Class 1 GPCP rainfall, (c) Class 2 OISST, (d) Class 2 GPCP rainfall, (e) Class 3 OISST, (f) Class 3 GPCP rainfall, (g) Class 4 OISST and (h) Class 4 GPCP rainfall. The black lines indicate scores significant at the 90% confidence level of a Student's  $t$ -test.

relationship with reduced East African long rains, perhaps through a Matsuno-Gill-like response (Hoell and Funk, 2014; Liebmann *et al.*, 2014).

Lyon (2014) found that the recent decrease in East African long rains was expressed in the largest decrease in April and May, a period during which wet regimes 1 and 2 as well as dry regime 3 are less frequent ( $-50$ ,  $-7$  and  $-12$  from Table 3, respectively), while dry regime 4 shows the highest increase ( $+69$ ). In conclusion, the abrupt decline of East African long rains after 1999 appears to be related, at intra-seasonal time scales, to modulations of the seasonal cycle as seen by significant shifts in prevailing convection regimes. Less frequent wet regime 1 occurrences in March–April and the highest frequencies of dry regime 4 in May suggest their respective primary contributions to regional drying in March–April and May respectively.

The largest seasonal frequency changes for regimes 1 and 3 (Table 3) together with substantial modulations of their respective persistence, that is, shorter-/longer-lived related episodes, respectively (Figure 9), further illustrate that equatorial Pacific SST changes have had a great influence in the post-1999 shift.

## 6. Discussion and conclusions

The main objective of this study was to identify sub-seasonal rainfall patterns linked to variability of East African rainfall during the MAM season and associate them with SST and circulation features. To this end, daily OLR data was used as a proxy for convection, which we examined through dynamical clustering ( $k$ -means) applied over the 1979–2013 period. Four dominant OLR

Table 3. Monthly count and total differences in the numbers of occurrences of the four NOAA daily OLR classes between the 1984–1998 and 1999–2013 periods<sup>a</sup>.

	Class 1	Class 2	Class 3	Class 4
1984–1998				
March	88	150	98	129
April	110	123	87	130
May	80	99	171	115
1999–2013				
March	52	101	196	116
April	78	107	130	135
May	62	108	116	179
1999–2013 minus 1984–1998				
March	–36 (–11.7)	–49 (–17.9)	+98 (+34.1)	–13 (–4)
April	–32 (–11.6)	–16 (–5.3)	+43 (+12.5)	+5 (+1.6)
May	–18 (–5.6)	+9 (+2.7)	–55 (–19.8)	+64 (+23.1)
Total	–86	–56	+86	+56

<sup>a</sup>The changes weighted by the ratio of monthly versus total seasonal occurrences shown in Table 2 are indicated for each class in brackets.

classes were identified. Regimes associated with wet conditions in East Africa (regimes 1 and 2) are found to preferentially occur at the beginning of the season (March and April) and are associated with low-level easterly wind anomalies over the IO at equatorial latitudes, a condition favouring enhanced moisture advection and local convergence. The other two regimes, especially regime 4, are associated with reduced rainfall over East Africa. Regime 4, related to significant drying, preferentially occurs at the end of the long rains season (in May) when the Somali jet is established along the East African coast, feeding in the Indian monsoon.

Regime 1 is found to be related to SST anomalies reminiscent of El Niño and accompanied by a V-like pattern of negative anomalies in the western extratropics of the Pacific, similar to the West Pacific Warm Mode discussed by Funk and Hoell (2015), the overall SST changes agreeing with the pattern identified by Lyon and DeWitt (2012). Regime 3 exhibits almost opposite relationships with SSTs but with less magnitude. Its impact on East African long rains is weaker than that of regime 4, with rainfall significantly reduced/enhanced in the central Pacific/over the MC. These precipitation anomalies are similar to those from La Niña, whose episodes in 1999, 2000 and 2008 were accompanied by increased frequencies and the persistence of this regime. Regime 2 and 4 generally display similar but oppositely signed SST anomaly patterns, particularly in the Pacific, where they show some similarity to ENSO precursors (Chang *et al.*, 2007) or perhaps ENSO Modoki, for which the peak warming is confined to the central equatorial Pacific until boreal winter instead of propagating to the east (Ashok *et al.*, 2007).

Overall, the dry regimes are related to almost opposite SST anomaly patterns in the Indo-Pacific than wet regimes. Similar results are found for precipitation anomaly composites for these regimes. In terms of associated circulation anomalies, wet regimes 1 and 2 generally show enhanced low-level moisture flux into East Africa associated with

corresponding divergence over the MC with anomalous easterly (westerly) fluxes across the equatorial Indian (Pacific) Ocean. Over the west IO, the anomalous easterly flux for these wet regimes acquires a southerly component along the East African coast. Dry regime 3 shows a generally opposite moisture flux pattern, with southerly flow off the East African coast and convergence into the eastern IO rather than the MC. A re-curving south-easterly flux into East Africa is seen in regime 4, with equatorial flux convergence further to the east than for regime 3 in the west Pacific. Regime 4 is of particular interest because of the recent drying in East Africa. Most frequent in May, it is associated with the establishment of the Somali jet along the East African coast, acting to enhance moisture divergence locally. The end of the long rains is thus concomitant with the start of the Indian monsoon.

In terms of the recent shift in East African rainfall, the individual daily OLR regimes do not occur with the same frequency before and after 1999. The number of occurrences of wet regimes has systematically decreased, while that of dry regimes has increased, particularly regime 4 during April and May when the largest East African precipitation declines are observed (Lyon and DeWitt, 2012). Because all regimes are associated with the SST gradient between the MC and the central Pacific, the modulations in their frequencies of occurrences can be related to the recent west Pacific warming/central Pacific cooling that has affected East African long rains (Lyon and DeWitt, 2012; Funk *et al.*, 2014a; Lyon, 2014). The increase in the west Pacific SSTs also has a contribution from longer-term trends (Hoell and Funk, 2014). In April and May, however, while the frequency of regimes 1, 2 and 3 decreased, the number of occurrences of dry regime 4 exhibited the largest increase compared to the pre-1999 time period, with associated episodes being more persistent. These transitions likely combine influences from the equatorial west and central Pacific (regimes 1, 2 and 4) and influences from a region near Hawaii (regimes 3 and 4), with the Indo-Pacific Walker circulation producing similar drought-inducing responses from these quite different SST forcing patterns. Of particular interest, associations between warming in the west Pacific subtropics and a more frequent dry regime 4 in May suggest that the recent drying in East Africa is related to an earlier onset of the monsoon and Somali jet, which is likely triggered by multi-decadal variability in the Pacific.

In conclusion, the results presented provide a useful framework to investigate the interactions between various convection regimes and other modes of atmospheric variability known to influence East African rainfall at multiple time scales (e.g. the MJO and the Pacific Decadal Oscillation). Such an approach reveals relationships that may contribute to the enhanced predictability of the East African long rains, possibly on the sub-seasonal time scale when non-linearities with Pacific and IO SSTs are taken into account. The next step, which is beyond the scope of this study, would be to further examine these potentials through modelling experiments.

## Acknowledgements

This work was supported by funding from the National Science Foundation project AGS 12-52301 on East African droughts. The Climate Hazards group InfraRed Precipitation with Station dataset (CHIRPS) was obtained from the University of California at Santa Barbara (USC) Climate Hazards Group (CHG) through the IRI Data Library (<http://iridl.ldeo.columbia.edu>), which was used extensively to also access daily atmospheric fields from NCEP-DOE II re-analyses and NOAA Optimum Interpolation SST version 2 (OISST).

## References

- Adler R, Huffman G, Chang A, Ferraro R, Xie P, Janowiak J, Rudolf B, Schneider U, Curtis S, Bolvin D, Gruber A, Susskind J, Arkin P. 2003. The version 2 global precipitation climatology project (gpcp) monthly precipitation analysis (1979-present). *J. Hydrometeorol.* **4**: 1147–1167.
- Affi T, Liwenga E, Kwezi L. 2014. Rainfall-induced crop failure, food insecurity and out-migration in same-Kilimanjaro, Tanzania. *Clim. Dev.* **6**(1): 53–60.
- Ashok K, Behera S, Rao S, Weng H, Yamagata T. 2007. El Niño Modoki and its possible teleconnection. *J. Geophys. Res. Oceans* **112**: 1–27, doi: 10.1029/2006JC003798.
- Behera S, Luo J, Mason S, Delecluse P, Gualdi S, Navarra A, Yamagata T. 2005. Paramount impact of the Indian Ocean dipole on the East African short rains: a CGCM study. *J. Clim.* **18**: 4514–4530.
- Beltrando G. 1990. Space-Time variability of rainfall in April and October–November over East Africa during the period 1932–1983. *Int. J. Climatol.* **10**: 691–702.
- Beltrando G, Camberlin P. 1993. Interannual variability of rainfall in the eastern horn of Africa and indicators of atmospheric circulation. *Int. J. Climatol.* **13**: 533–546.
- Berhane F, Zaitchik B. 2014. Modulation of daily precipitation over East Africa by the Madden-Julian Oscillation. *J. Clim.* **27**: 6016–6034, doi: 10.1175/JCLI-D-13-00693.1.
- Camberlin P, Okoola R. 2003. The onset and cessation of the long rains in eastern Africa and their inter annual variability. *Theor. Appl. Climatol.* **75**: 43–54.
- Camberlin P, Philippon N. 2002. The East African March–May rainy season: associated atmospheric dynamics and predictability over the 1968–97 period. *J. Clim.* **15**: 1002–1019.
- Chang P, Zhang L, Saravanan R, Vimont D, Chiang J, Ji L, Seidel H, Tippet M. 2007. Pacific meridional mode and El Niño–Southern Oscillation. *Geophys. Res. Lett.* **34**: 1–5, doi: 10.1029/2007GL030302.
- Cheng X, Wallace J. 2003. Regime analysis of the Northern Hemisphere winter-time 500 hPa height field: spatial patterns. *J. Atmos. Sci.* **50**: 2674–2696.
- Fauchereau N, Pohl B, Reason C, Rouault M, Richard Y. 2009. Recurrent daily OLR patterns in the Southern Africa/Southwest Indian Ocean region, implications for South African rainfall and teleconnections. *Clim. Dyn.* **32**: 575–591.
- Funk C, Hoell A. 2015. The leading mode of observed and CMIP5 ENSO-Residual sea surface temperatures and associated changes in Indo-Pacific climate. *J. Clim.* **28**: 4309–4329.
- Funk C, Dettinger M, Michaelsen J, Verdin J, Brown M, Barlow M, Hoell A. 2008. Warming of the Indian Ocean threatens eastern and southern African food security but could be mitigated by agricultural development. *Proc. Natl. Acad. Sci. U. S. A.* **105**: 11081–11086, doi: 10.1073/pnas.0708196105.
- Funk C, Hoell A, Shukla S, Liebmann B, Roberts J, Robertson F, Husak G. 2014a. a ), Predicting East African spring droughts using Pacific and Indian Ocean sea surface temperature indices. *Hydrol. Earth Syst. Sci. Discuss.* **11**: 3111–3136.
- Funk C, Peterson P, Landsfeld M, Pedreros D, Verdin J, Rowland J, Romero B, Husak G, Michaelsen J, Verdin A. 2014b. A quasi-global precipitation time-series for drought monitoring. *US Geological Survey Data Series*, 832: 4 pp.
- Funk C, Nicholson S, Landsfeld M, Klotter D, Harrison L. 2015a. The centennial trends Greater Horn of Africa precipitation dataset. *Sci. Data* **2**: 1–15, doi: 10.1038/sdata.2015.50.
- Funk C, Peterson P, Landsfeld M, Pedreros D, Verdin J, Shukla S, Husak G, Rowland J, Harrison L, Hoell A, Michaelsen J. 2015b. The climate hazards infrared precipitation with stations—a new environmental record for monitoring extremes. *Sci. Data* **2**: 1–21, doi: 10.1038/sdata.2015.66.
- Goddard L, Graham N. 1999. The importance of the Indian Ocean for simulating precipitation anomalies over eastern and southern Africa. *J. Geophys. Res.* **104**: 19099–19116.
- Hastenrath S, Niklis A, Greischar L. 1993. Atmospheric-hydrospheric mechanisms of climate anomalies in the Western equatorial Indian Ocean. *J. Geophys. Res.* **98**: 219–235.
- Hession S, Moore N. 2011. A spatial regression analysis of the influence of topography on monthly rainfall. *Int. J. Climatol.* **31**: 1440–1456.
- Hoell A, Funk C. 2014. Indo-Pacific sea surface temperature influences on failed consecutive rainy season over eastern Africa. *Clim. Dyn.* **43**: 1645–1660.
- Indeje M, Semazzi F, Ogallo L. 2000. ENSO signals in East African rainfall seasons. *Int. J. Climatol.* **20**: 19–46.
- Kanamitsu M, Ebisuzaki W, Woollen J, Yang S-K, Hnilo J, Fiorino M, Potter GL. 2002. Ncep-doe amp-2 reanalysis (r-2). *Bull. Am. Meteorol. Soc.* **83**: 1631–1643.
- Liebmann B, Smith C. 1996. Description of a complete (interpolated) outgoing longwave radiation dataset. *Bull. Am. Meteorol. Soc.* **83**: 1631–1643.
- Liebmann B, Blade I, Kiladis G, Carvalho L, Senay G, Allured D, Leroux S, Funk C. 2012. Seasonality of African precipitation from 1996 to 2009. *J. Clim.* **25**: 4304–4322.
- Liebmann B, Hoerling M, Funk C, Blade I, Dole R, Allured D, Quan X, Pegion P, Eischeid J. 2014. Understanding the Eastern Horn of Africa rainfall variability and change. *J. Clim.* **27**: 8630–8645.
- Lyon B. 2014. Seasonal drought in East Africa and its recent increase during the March–May long rains. *J. Clim.* **27**: 7953–7975.
- Lyon B, DeWitt D. 2012. A recent and abrupt decline in the East African long rains. *Geophys. Res. Lett.* **39**: 1–5, doi: 10.1029/2011GL050337.
- Lyon B, Barnston A, DeWitt D. 2014. Tropical Pacific forcing of a 1998–99 climate shift: observational analysis and climate model results for the boreal spring season. *Clim. Dyn.* **43**: 893–909.
- Mason S. 1995. Sea-surface temperatures–South African rainfall associations. *Int. J. Climatol.* **15**: 119–135.
- Michelangeli P, Vautard R, Legras B. 1995. Weather regime occurrence and quasi-stationarity. *J. Atmos. Sci.* **52**: 1237–1256.
- Moron V, Plaut G. 2003. The impact of El Niño–Southern Oscillation upon weather regimes over Europe and the North Atlantic during boreal winter. *Int. J. Climatol.* **23**: 363–379.
- Moron V, Camberlin P, Robertson A. 2013. Extracting sub-seasonal scenarios: an alternative method to analyze seasonal predictability of regional-scale tropical rainfall. *J. Clim.* **26**: 2580–2600.
- Mutai C, Ward M. 2000. East African rainfall and the tropical circulation/convection on intraseasonal to interannual timescales. *J. Clim.* **13**: 3915–3939.
- Nicholson SE. 2014. The predictability of rainfall over the Greater Horn of Africa. Part I: prediction of seasonal rainfall. *J. Hydrometeorol.* **15**: 1011–1027.
- Nicholson SE. 2015. Short communication: an analysis of recent rainfall conditions in eastern Africa. *Int. J. Climatol.* **36**: 526–532, doi: 10.1002/joc.4358.
- Ogallo L. 1988. Relationships between seasonal rainfall in East Africa and the Southern Oscillation. *Int. J. Climatol.* **8**: 31–43.
- Ogallo L, Janowiak J, Halpert M. 1988. Teleconnections between seasonal rainfall over East Africa and global sea surface temperature anomalies. *J. Meteorol. Soc. Jpn.* **66**: 807–822.
- Okoola R. 1999. A diagnostic study of Eastern African monsoon circulation during the northern hemisphere spring season. *Int. J. Climatol.* **19**: 143–168.
- Omondi P, Ogallo L, Anyah R, Muthama J, Ininda J. 2013. Linkages between global sea surface temperatures and decadal variability over East Africa region. *Int. J. Climatol.* **33**: 2082–2104.
- Peixoto J, Oort A (eds). 1992. *Physics of Southern African Climate*. Springer-Verlag, 520 pp.
- Philipps A, McIntyre B. 2000. ENSO and interannual variability in Uganda: Implications for agricultural management. *Int. J. Climatol.* **20**: 171–182.
- Pohl B, Camberlin P. 2006a. Influence of the Madden-Julian Oscillation on East African rainfall. Part I: intraseasonal variability and regional dependency. *Q. J. R. Meteorol. Soc.* **132**: 2521–2539.
- Pohl B, Camberlin P. 2006b. Influence of the Madden-Julian Oscillation on East African rainfall. Part II: March–May season extremes and inter-annual variability. *Q. J. R. Meteorol. Soc.* **132**: 2541–2558.

- Pricope N, Husak G, Lopez-Carr D, Funk C, Michaelsen J. 2013. The climate-population nexus in the East African Horn: emerging degradation trends in rangeland and pastoral livelihood zones. *Glob. Environ. Change* **23**: 1525–1541.
- Reynolds RW, Smith TM, Liu C, Chelton D, Casey K, Schlax M. 2007. Daily high-resolution-blended analyses for sea surface temperature. *J. Clim.* **20**: 5473–5496.
- Riddle E, Cook K. 2008. Abrupt rainfall transitions over the Greater Horn of Africa: Observations and regional model simulations. *J. Geophys. Res.* **113**: 1–14, doi: 10.1029/2007JD009202.
- Shukla S, McNally A, Husak G, Funk C. 2014. Seasonal drought forecast system for food-insecure regions of East Africa, In *EGU General Assembly Conference Abstracts*, 16.
- Verdin J, Funk C, Senay G, Choularton R. 2005. Climate science and famine early warning. *Philos. Trans. R. Soc. B* **360**: 2155–2168.
- Vigaud N, Richard Y, Rouault M, Fauchereau N. 2007. Water vapour from the tropical Atlantic and summer rainfall in tropical southern Africa. *Clim. Dyn.* **28**: 113–123, doi: 10.1007/s00382-006-0186-9.
- Vigaud N, Richard Y, Rouault M, Fauchereau N. 2009. Moisture transport between the South Atlantic Ocean and southern Africa: relationships with summer rainfall and associated dynamics. *Clim. Dyn.* **32**: 113–123, doi: 10.1007/s00382-008-0377-7.
- Vigaud N, Pohl B, Cretat J. 2012. Tropical-temperate interactions over southern Africa simulated by a regional climate model. *Clim. Dyn.* **39**: 2895–2916, doi: 10.1007/s00382-012-1314-3.
- Viste E, Korecha D, Sorteberg A. 2011. Recent drought and precipitation tendencies in Ethiopia. *Theor. Appl. Climatol.* **112**: 535–551, doi: 10.1007/s00704-012-0746-3.
- Vizy E, Cook K. 2003. Connections between the summer East African and Indian rainfall regimes. *J. Geophys. Res.* **108**: 1–19, doi: 10.1029/2003JD003452.
- Walker N. 1990. Links between South African summer rainfall and temperature variability of the Agulhas and Benguela current systems. *J. Geophys. Res.* **95**: 3297–3319.
- Williams A, Funk C. 2011. A westward extension of the warm pool leads to a westward extension of the Walker circulation, drying eastern Africa. *Clim. Dyn.* **37**: 2717–2435.
- Yang W, Seager R, Cane M, Lyon B. 2014. The East African long rains in observations and models. *J. Clim.* **27**: 7185–7202, doi: 10.1175/JCLI-D-13-00447.